GA–A21851

DIVERTOR RESEARCH ON THE DIII–D TOKAMAK

by
D.N. HILL,* S.L. ALLEN,* N.H. BROOKS, D. BUCHENAUER,† J.W. CUTHBERTSON,‡ T.E. EVANS, M.E. FENSTERMACHER,* Ph. GHENDRIH,△ D.L. HILLIS,◊ J.T. HOGAN,◊ A.W. HYATT, G.L. JACKSON, R.A. JAMES,* R. JONG,* C.J. LASNIER,* A.W. LEONARD, M.A. MAHDAVI, R. MAINGI,# M.M. MENON,◊ P.K. MIODUSZEWSKI,◊ R.A. MOYER,‡ T.W. PETRIE, G.D. PORTER,* M.E. RENSINK,* M.J. SCHAFFER, G.M. STAEBLER, D.M. THOMAS, M.R. WADE,◊ J.G. WATKINS,† F. WESCHENFELDER,§ W.P. WEST, D. WHYTE,¶ and R. WOOD*

This is a preprint of a paper to be presented at the Fifteenth International Conference on Plasma Physics and Controlled Nuclear Fusion, September 26 through October 1, 1994, in Madrid, Spain, and to be published in the Proceedings.

Work supported by
U.S. Department of Energy
Contract Nos. W-7405-ENG-48, DE-AC03-89ER51114, DE-AC05-OR21400, DE-AC04-76DP00789, DE-FG03-89ER51121, and DE-FG03-86ER53225

*Lawrence Livermore National Laboratory
†Sandia National Laboratory
‡University of California at Los Angeles
△Association EURATOM-CEA, Cadarache, France
◊Oak Ridge National Laboratory.
#Oak Ridge Associated Universities
§KFA
¶CCFM

GENERAL ATOMICS PROJECT 3466
OCTOBER 1994

DISCLAIMER

DISCLAIMER

Portions of this document may be illegible in electronic image products. Images are produced from the best available original document.

IAEA-CN-60/A-4-I-2

DIVERTOR RESEARCH ON THE DIII–D TOKAMAK

ABSTRACT

In this paper we summarize recent progress on DIII–D in developing techniques for divertor power and particle control relevant to next generation tokamaks such as the proposed ITER and TPX devices. Density control and helium removal by divertor pumping have been demonstrated for the first time in high confinement ELMing H–mode discharges ($\tau \sim 2 \times \tau_{ITER\text{-}89P}$) following installation of a divertor cryopumping system. The peak divertor heat flux in similar H–mode discharges has been reduced through production of a radiating mantle with neon or argon puffing (reductions of 5–10) or by increasing the divertor-region radiation with deuterium puffing (reductions of 3–5). A number of diagnostics have been added to improve our understanding of the physical processes involved. We are now designing modified double-null divertor structures for DIII–D that will provide improved particle control for high-triangularity VH–mode plasmas while at the same time allowing for gas puffing to reduce the divertor heat flux.

1. INTRODUCTION

In this paper we summarize recent experiments in DIII–D that have focused on developing techniques for steady-state divertor power and particle control relevant to next generation tokamaks such as the proposed ITER and TPX devices. Power handling and particle control are key design issues for these new machines [1], and the tokamak community has readjusted its priorities to reflect these needs. In DIII–D we have installed a divertor cryopump to provide particle exhaust and density control in ELMing H–mode plasmas [2] and have used gas injection (impurities and deuterium) to reduce the peak target plate heat flux [3]. Deuterium puffing increases the plasma density and radiative losses in the divertor region near the X-point and can help keep impurities out of the core plasma, while impurity puffing generally forms a radiating mantle that reduces the power flow into the scrape-off layer (SOL). Our results show that achieving these plasma parameters does not require deep divertors, and that, once obtained, the conditions are stable over a wide range of high density, high confinement H–mode operating space ($\tau \sim 2 \times \tau_{ITER\text{-}89P}$), and offer the possibility of adequate helium ash exhaust. We believe that such operating modes offer a credible solution to power handling in ITER.

Extending these reduced heat flux operating modes to the lower plasma densities suitable for advanced tokamak regimes with non-inductive current drive is now the central focus of the DIII–D divertor program. Indeed, obtaining independent control of the divertor parameters for a given set of discharge conditions is the central challenge facing the divertor physcis community today. We are now designing a double-null divertor modification [4] to increase the isolation of deuterium and impurity gas between the divertor and main plasma and enhance the particle flow in the scrape-off layer, thereby decoupling the core and divertor plasma conditions in a controlled manner.

The principal results of our divertor studies are reported here as follows. In Section 2 we show how particle control has been obtained with the divertor cryopump. Section 3 then shows how our diagnostic improvements, coupled with the pump as a tool for changing recycling, have increased our understanding of the power balance in the scrape-off layer. Section 4 focuses on divertor heat flux reduction by gas injection, and Section 5 shows how we plan to extend this work in the Radiative Divertor Program.

2. PARTICLE CONTROL WITH DIVERTOR PUMPING

The installation of the divertor cryopump has provided a reliable means of particle control in DIII–D. The pumping hardware [5], Fig. 1(a), consists of a baffle to limit the escape of particles from the divertor region, an entrance slot (or pump throat) to direct recycled neutrals from the target plate toward the pump, and the liquid helium cooled cryopump. The top of the entrance slot (called the bias ring) can be electrically biased to draw current in the SOL plasma and enhance pumping by creating additional $E \times B$ ion drifts toward the throat [6]. The pumping speed of the pump, 35 m^3/s, is matched to the gas conductance of the entrance slot and it has sufficient capacity to pump for the 10 second duration of the discharge. Argon frosting of the cryopump surface allows for helium pumping as well [5].

The particle exhaust rate with pumping depends on the particle flux at the outer divertor target and on the fraction of recycled neutrals which enter the pump throat. The flux increases with plasma density and heating power and is highest during ELMing H–mode operation. Maximum throughput under these conditions is obtained when the outer divertor strike point is positioned just inside the entrance slot, Fig. 1(b), where neutrals recycled from the divertor targets have the highest probability of heading into the

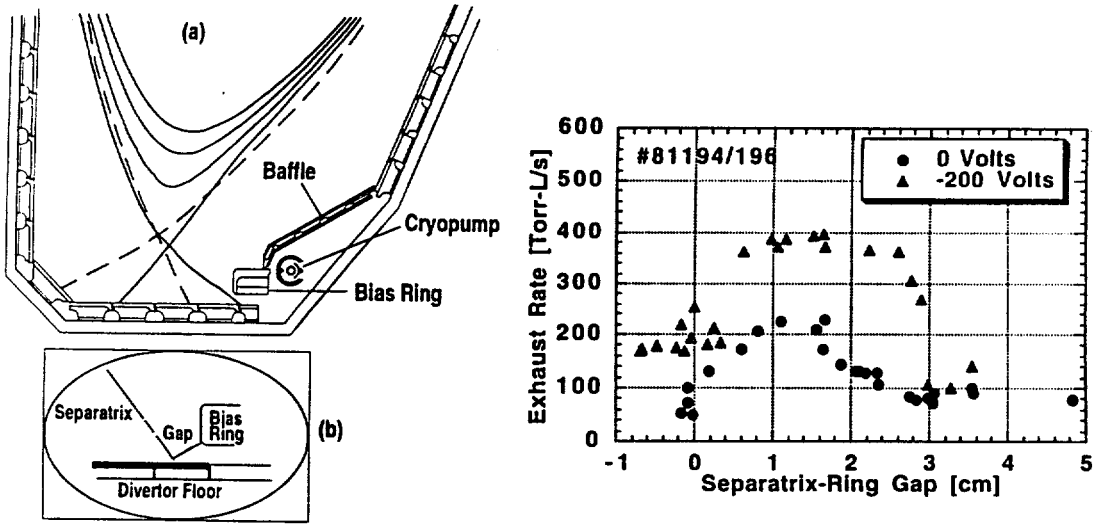

Fig. 1. (a) Cross section of DIII–D divertor region showing cryopump. (b) particle throughput vs. gap between the separatrix and the face of the pump entrance (or bias ring). Bias ring voltage as indicated.

plenum. The variation in exhaust rate with strike point position is consistent with the measured width of the scrape-off layer plasma in the divertor. Here the exhaust rate is determined from the measured plenum pressure and the known pumping speed: Q = SxP.

Operation of the divertor cryopump has provided a means for density control in high confinement H–mode plasmas for the first time. The data in Fig. 2(a) show typical behavior during pumping. After a rapid rise following the H–mode transition, the density gradually falls back to near the initial L–mode value. The minimum density obtained so far ($n_e \simeq 3\times10^{19}$ m^{-3}) has been limited by the onset of a locked mode, followed by a plasma disruption; field-error correction coils have been installed to lower this limit even further. The drop in density during pumping is accompanied by a rise in electron temperature, so that stored energy and confinement time remain independent of density [7]. The particle exhaust is highest during the ELMing phase because the ELMs are responsible for the bulk of the particle losses in these quasi steady state H–mode discharges [8].

Examination of the particle balance for discharges with pumping shows that the cryopump can control the gas inventory of the tokamak walls. This is an important feature for future steady-state operation in which glow discharge cleaning or other wall conditioning techniques may not be practical. Figures 2(b–e) show the particle balance (wall and plasma) during pumping. At first, the gas fueling increases the wall inventory of

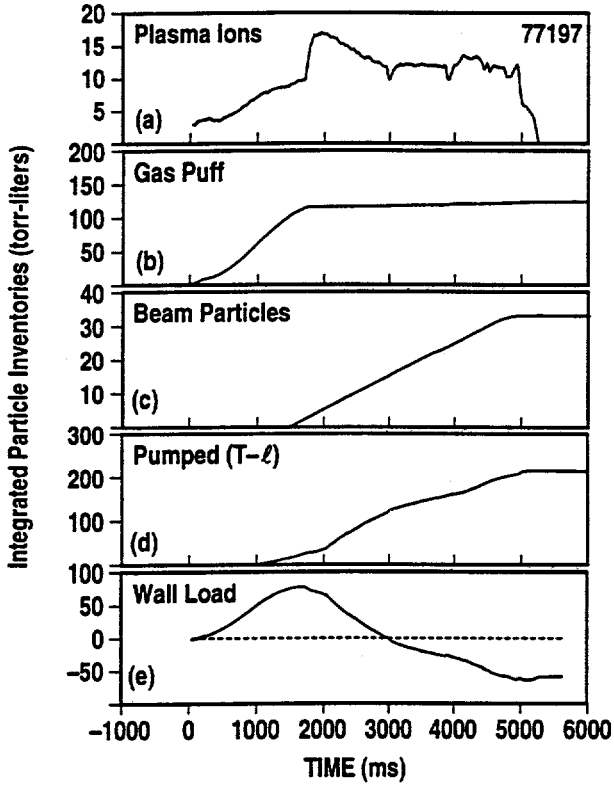

Fig. 2. Particle balance for divertor pumping. (a) particle inventory in plasma, (b) gas fueling, (c) particle source from neutral beams, (d) particle exhaust by cryo-pump, (e) net particle inventory remaining in vessel.

the well conditioned graphite surfaces. At the start of H–mode, the external fueling is sharply reduced and the plasma density builds due to fueling from the walls. Continued particle exhaust by the cryopump gradually depletes the wall so that, by the end of the pulse, there has been a net reduction in the particle content in the graphite wall [2].

Density control by divertor pumping is aided by divertor biasing, which increases the particle flux into the pump throat [9]. This may be particularly useful for low density non-inductive current drive experiments. We have found that biasing the outer leg of the divertor plasma negatively with respect to the vessel wall can increase the particle throughput by nearly a factor of two, as shown in Fig. 1(b). In this case, we expect that the applied voltage produces a radial electric field and a corresponding poloidal $E \times B$ plasma drift along the outer divertor leg. The data in Fig. 1(b) also show that biasing reduces the dependence of the throughput on the gap [10].

The divertor cryopump has also been used to exhaust thermal helium from ELMing H–mode discharges [11]. Helium pumping is obtained by coating the liquid helium cryopump with argon frost. The helium was introduced via gas puffing and was found to quickly redistribute to a nearly uniform concentration throughout the main plasma. It was found that the exhaust rate of helium from the plasma was limited by the exhaust efficiency of the pump, and not helium transport in the core plasma. The helium concentration in the pump plenum peaked when the separatrix intercept was in the pump throat and was in the range 10%–20% for a 15% core concentration.

3. SCRAPE-OFF LAYER STUDIES

Characterization of the scrape-off layer and divertor plasma scaling with main plasma parameters remains an important part of the DIII–D divertor program because it is essential for testing numerical models such as the b2 and UEDGE codes [12]. Benchmarking these 2–d codes really requires SOL profile measurements at several different poloidal locations to test the transport models, as there are enough degrees of freedom in the problem to allow for a reasonable match to the data at any single location. We find that the UEDGE code can reproduce the measured midplane and divertor profiles using diffusion coefficients in the range $0.05 \leq D_{\perp} \leq 0.25$ m/s and $0.1 \leq \chi_{\perp} \leq 0.25$ m^2/s. A detailed report on modeling the DIII–D scrape off layer with UEDGE is presented elsewhere [13].

Foremost among the parameters essential to modeling the scrape off layer plasma is the power balance, as this defines how the energy is transported from the plasma to the walls. The power balance of ELMing H–mode discharges in DIII–D has been improved significantly by the addition of new bolometer cameras [14] to better resolve the radiative losses (including the contributions due to ELMs) and by monitoring the heat flux on the inner wall and other non-divertor surfaces using additional IR TV cameras. We now can account for about 70%–85% of the total input power for ELMing H–mode discharges [15], and find that about 20% is lost as radiation in the main plasma, 40%–50% as radiation in the divertor region, and only about 15% reaches the divertor targets, independent of the heating power.

Local power balance measurements in the divertor, summarized in Table 1, show that radiation asymmetries are responsible for the large in/out poloidal asymmetries in the target plate heat flux observed when the ion ∇B drift is toward the X-point. Inversion of the bolometer data shows that nearly 75% of the divertor radiation comes from along the inner

divertor leg, and this energy loss reduces the power conducted to the inner target plate to <5% of the total heating power. In fact, about half the heat flux measured at the inner strike point is due to radiative heating. The opposite situation is true for the outer leg (low radiation, high heat flux). So, in fact, the total power flow in the scrape-off layer is more equally divided between the inner and outer divertor legs [15] than is suggested by the heat flux data only. This is consistent with numerical modeling which showed that the in/out asymmetry was only weakly dependent on the poloidal location of the power flux across the separatrix, due to the high thermal conductivity of the scrape off layer plasma [16].

The large radiative loss on the inner divertor leg allows the scrape-off layer plasma to detach from the inner target plate; i.e., pressure balance and its consequences for SOL scaling no longer hold. Evidence for this comes from the Langmuir probes and divertor heat flux measurements, Fig. 3. Here we have used the divertor cryopump to vary the line average density and radiative losses on the inner divertor leg [17]. As the main plasma density rises, the particle flux at the inner leg increases and the electron temperature decreases, as it should if the plasma pressure is constant along field lines [18]. Above 4×10^{19} m^{-3}, however, the particle flux sharply decreases, as in (a), and the heat flux profile broadens to the point where, at 7×10^{19} m^{-3}, we can no longer relate the inner and outer heat flux profiles using electron heat conduction and field line mapping, (b).

Other studies of the divertor conditions in DIII–D have examined the issues of toroidal asymmetries, impurity transport [19], and scrape-off layer broadening [20]. In general, using data from two toroidally separated IR TVs, we find that toroidal asymmetries in steady-state single-null divertor heat flux are rare (≤5% of H–mode discharges) [21]. The one exception to this is when locked modes are present, and in this case the asymmetries manifest themselves as toroidally varying radial modulations in the heat flux profile (multiple peaks separated by cm) with little (≤20%) variation in the peak divertor heat flux. Transient n=1 toroidal asymmetries during ELMs have been observed in net current flow to the inner target plate tiles.

TABLE I. Power balance for ELMing H–mode discharges

Loss Channel	% of Heating Power	
Core radiation	18	
Inner-wall heat flux	5	
	Inner Divertor	Outer Divertor
Divertor radiation	22	19
Target-plate heat flux	3	27
Total divertor	25	37
Total measured losses	85	

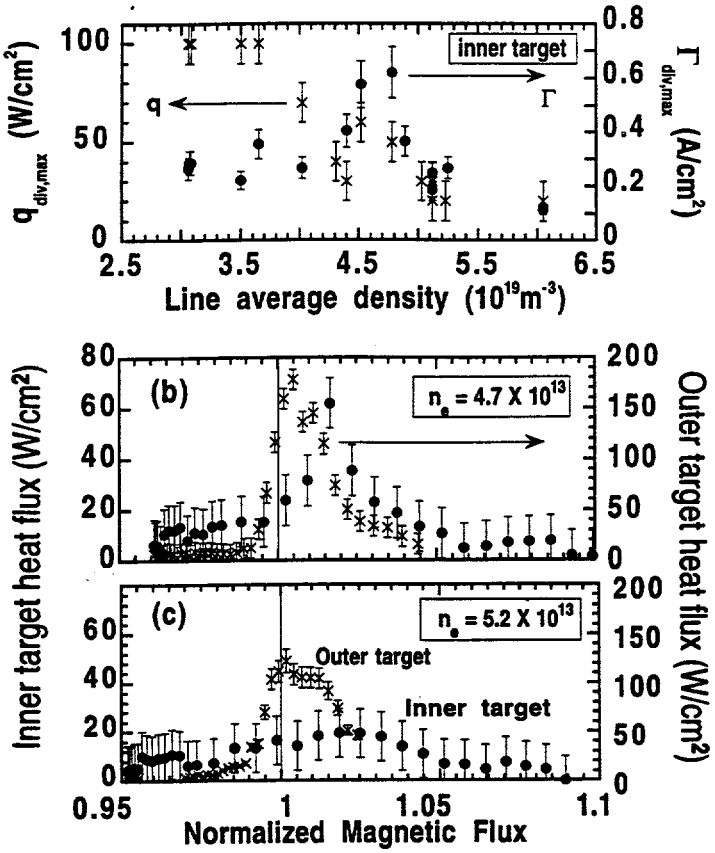

Fig. 3. Plasma detachment at the inner divertor. (a) variation of divertor heat and particle flux with density. Heat flux profiles mapped to midplane for (b), $\bar{n}_e = 4.7\times10^{19}\ m^{-3}$ *(b), and* $5.2\times10^{19}\ m^{-3}$ *(c).*

4. DIVERTOR HEAT FLUX REDUCTION

Future long–pulse high power tokamaks will require that the *peak* divertor heat flux be reduced by factors of 10 or more from values predicted using present models or scaling relations. Tilting the target plates can yield a factor of three reduction, but further reduction will require that a significant fraction of the heating power be radiatively dissipated before it is conducted to the divertor targets. Experiments with ELMing H–mode plasmas in DIII–D have focused on two possible means of increasing the radiated fraction above naturally occurring levels: deuterium injection to increase the divertor radiation by raising the divertor density (increasing the recycling), and impurity injection to raise the radiative efficiency of the SOL/divertor plasma. With D_2 puffing, the peak divertor heat flux was reduced by a factor of 3–5 and the divertor plasma partially detached following the appearance of a divertor Marfe near the X–point [22]. Neon injection [4] produced a radiating mantle in the main plasma which reduced power flow across the separatrix and dropped the peak divertor heat flux by factors of 5–10. We have now begun to examine if

divertor pumping combined with gas puffing (D_2 and impurities) might be used to increase the fraction of power radiated by neon in the divertor region or provide divertor cooling at lower line-average density.

4a. Detached divertor plasmas with deuterium puffing

Recently, operation with reduced peak divertor heat flux (factor of four) and continuous particle exhaust by the cryopump has been maintained for the duration of the gas pulse (~2 s), as shown in Fig. 4. In this case, the outer divertor strike point was held near the pump throat while deuterium was injected below the X-point. The exhaust rate matched the fueling rate (180–240 torr-l/s out vs. 210 torr-l/s in) so that the plasma density remained nearly constant, though at about the same density as normally obtained without pumping. This condition was very stable, requiring virtually no feedback control of the gas puff even though 75% of the input power was being radiated.

In these partially detached divertor plasmas, the radiative losses are localized on the outer divertor leg near the X-point, as shown by the 2-d reconstruction of bolometer data, Fig. 5. The region of high radiation appears to extend down the outside divertor leg somewhat (also evident in X-point TV images with a CIII filter), but exact placement is

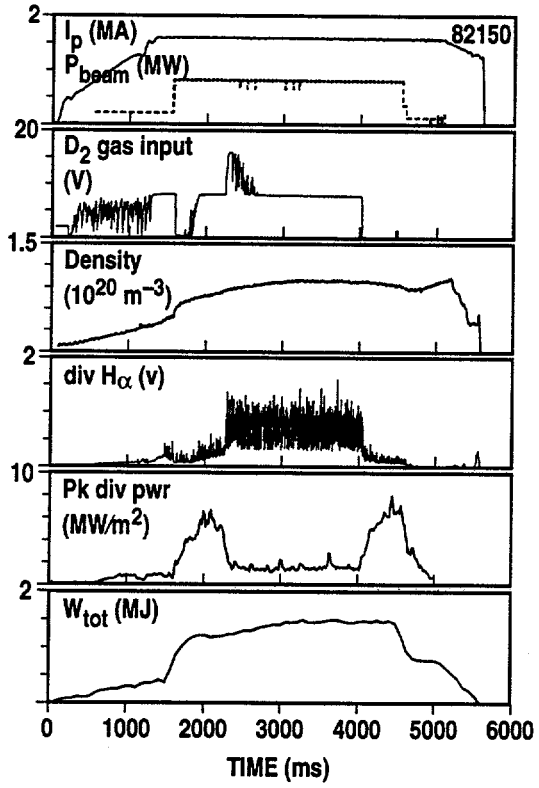

Fig. 4. Deuterium gas injection with divertor pumping. (a) solid-plasma current and dashed-beam power, (b) D_2 fueling rate, (c) plasma density, (d) H_α at outer divertor target, (e) peak divertor heat flux, (f) total stored energy.

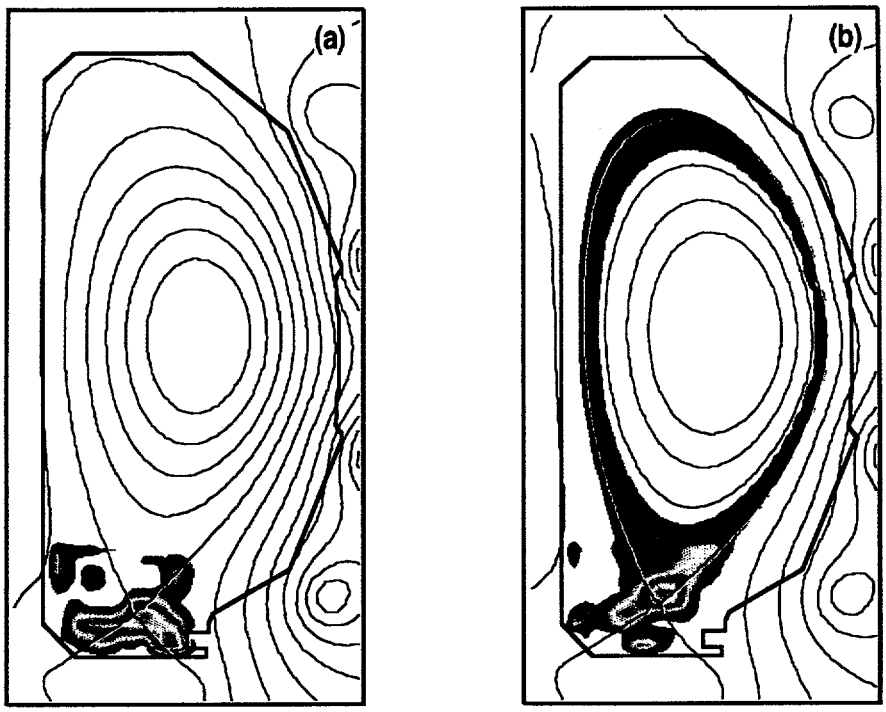

Fig. 5. 2-d spatial distribution of radiative losses with D_2 puff (a) and neon puff (b) to reduce divertor heat flux. Peak emissivities are 5.5 MWm^{-3} for D_2 and 2MWm^{-3} for neon.

limited by the finite number of viewing chords and directions. We believe that this region of localized radiation is a Marfe-like thermal condensation [23], because interferometer measurements suggest that the local plasma density may be as much as ten times higher than elsewhere in the edge plasma and because of its rapid formation (≤5 ms). The Marfe appears when the neutral pressure in the private flux region exceeds a critical value which increases linearly with SOL power [24]. Conditions suitable for Marfe formation are attained when the main plasma density is at or above a significant fraction (0.7–0.8) of the Greenwald density limit. This fraction is independent of the heating power in clean ($Z_{eff} < 2$) discharges, Fig. 6(a).

The divertor Marfe is stable over a wide range of operating conditions in DIII–D and does not significantly reduce confinement (τ_E ~2×L–mode) nor increase the impurity content of the main plasma. In fact, during the strong gas puffing Z_{eff} drops as the ELM frequency increases. It is controllable over a wide range of safety factors ($2.9 \le q_{95} \le 6$) and heating powers (3.6–20 MW) and does not require a deep divertor to form (L_{div} = 0.05–0.25 m). It can be sustained by minimal gas fueling from either the private region below the X-point or the midplane (the fueling rate is comparable to ion loss rate from the main plasma, N/τ_p, which is much less than the initial ion flux at the divertor plate). One

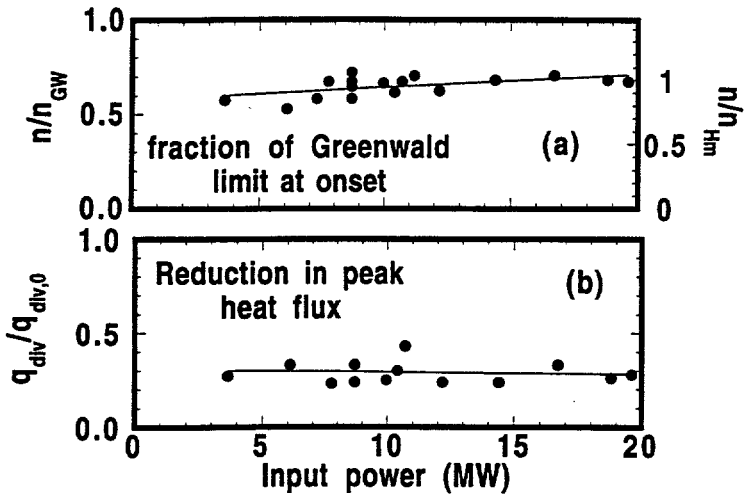

Fig. 6. Power scaling of partially detached plasmas with a divertor Marfe. (a) Minimum density for Marfe formation, where $\bar{n}_{GW} = \kappa \bar{J}$ *(*10^{20} *m–3) =* $I/\pi a^2$ *(in MA/m*^{2}*) is in the Greenwald density limit and* $\bar{n}_{\text{H-mode}} n$ *is the typical density for H–mode plasmas in DIII–D:* n_{H-mode} *(*10^{20} m^{-3}*)* $\simeq$ *0.7* $\bar{n}_{GW} \cong 0.6\, I_p$ *(MA). (b) reduction in peak divertor heat flux vs power.*

attractive feature of this operating mode is that it reduces the heat flux peaking factor ($\hat{q}_{div}/P_{target}$) by about a factor of two, thus reducing the thermally induced mehcanical stress for a given total radiation loss. This reduction in peak heat flux is independent of heating power, Fig. 6(b).

4b. Operation with impurity puffing

Impurity puffing into DIII–D ELMing H–mode plasmas can reduce the peak divertor heat flux by a factor of ten or more. In these plasmas, short pulses (5–100 ms) of neon or argon gas below the X-point in DIII–D produce steady-state radiation profiles like those shown in Fig. 5(b) and 7(a). The bright region near the X-point is responsible for nearly half the total impurity radiation; we are not sure why this is so, since there are no indications of higher plasma density (a Marfe) there. The measured emissivity in the main plasma is consistent with the expected radiation for a uniform 3% neon concentration in the main plasma, which agrees with charge-exchange recombination and Z_{eff} measurements. This amount of neon corresponds to about 50% of the total neon injected into the vessel.

In contrast to deuterium puffing, the radiative losses in this case cool the edge plasma inside the separatrix and reduce the power flow into the scrape-off layer, Fig. 7(b,c). A cooler scrape-off layer plasma results. As a consequence, the density, temperature, and heat flux at the divertor target are reduced significantly, just as they would be if the external heating power were reduced. This is fundamentally different than the detached plasma, where the upstream plasma pressure on, and heat flux across, the separatrix remain high.

Reducing the power flow across the separatrix also affects ELM behavior. We have observed that neon and argon puffing can reduce the ELM frequency by more than a factor

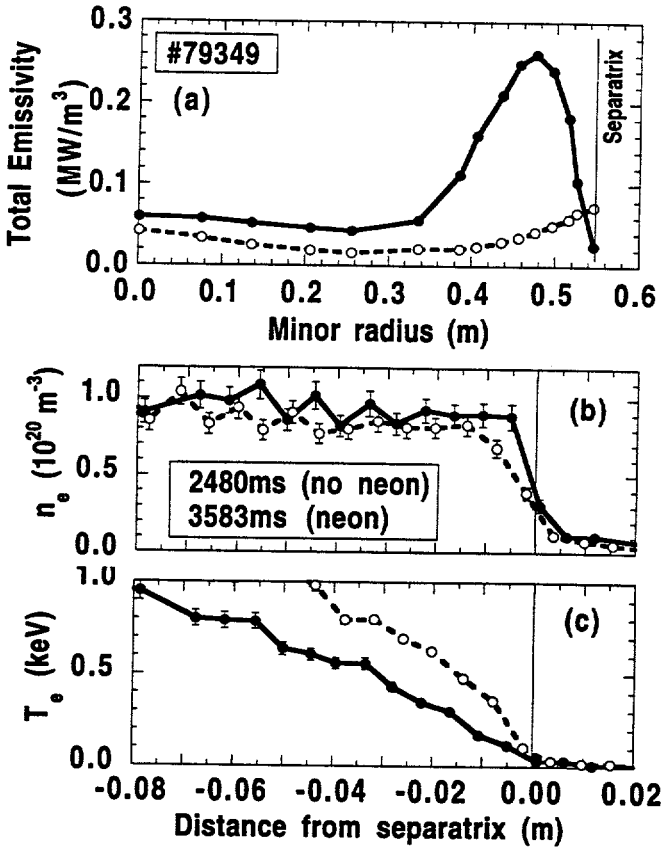

Fig. 7. Midplane radial profiles for neon injection experiments. (a) measured total emissivity—separatrix is at 0.55m, (b) electron temperature, (c) electron density. Dashed traces are without neon puff.

of ten, producing very large ELMs (greater than 10% changes in stored energy at each ELM). Additional impurity input reduces the power reaching the separatrix even further, producing small Type III ELMs when it drops near the H–mode power threshold. One consequence of reducing the ELM frequency may be that impurity confinement increases, This implies that helium exhaust could be more difficult. More study is needed.

Reducing the power flow across the separatrix also affects ELM behavior. We have observed that neon and argon puffing can reduce the ELM frequency by more than a factor of ten, producing very large ELMs (greater than 10% changes in stored energy at each ELM). Additional impurity input reduces the power reaching the separatrix even further, producing small Type III ELMs when it drops near the H–mode power threshold. One consequence of reducing the ELM frequency may be that impurity confinement increases, This implies that helium exhaust could be more difficult. More study is needed.

The radiating mantle produced by neon injection (similar results were also obtained with argon injection, though the central radiation was higher in that case) also favors high density operation since the radiative losses scale as $L(T)C\,n_e^2$, where C is the impurity

concentration and L(T) is the radiative efficiency for a given impurity and plasma temperature profile. Thus, it may not be compatible with advanced tokamak regimes (high confinement, high β_N) requiring low density for non-inductive current profile control. We are now testing methods for enhancing the impurity content and radiative losses in the divertor compared to the main plasma in order to make large heat flux reduction possible at relatively lower density.

4c. Simultaneous impurity and deuterium injection with divertor pumping

Divertor pumping, combined with main plasma fueling may increase particle flow in the scrape-off layer and improve impurity retention in the divertor region. Positioning the divertor strike point near the throat of the cryopump in DIII–D may also minimize the leakage of impurities out of the divertor. Preliminary experiments with argon injection [25] showed that a strong reduction in core Ar concentration could be maintained for the duration of the plasma pulse by simultaneously fueling with D_2 near the midplane and pumping with the divertor cryopump. Exact particle balance was not maintained, however, since $\bar{n}_e$ rose by bout 30%. Without the divertor pumping and deuterium injection, the argon levels rose to the disruptive limit in <0.5 s.

Experiments with perturbing levels of impurity injection and divertor pumping are now under way. Figure 8 shows data from a discharge with neon injection in the divertor, high deuterium fueling at the midplane (~150 torr-l/s), and modest divertor pumping (G_{pump} ~ 120 torr-l/s). In this case, the D_2 fueling was controlled by the density feedback system and the neon injection rate was gradually increased to determine its effect on the divertor heat flux. As shown in (c), by 2.7 s the peak divertor heat flux was reduced by more than a factor of five while Z_{eff} had changed little. Inversion of the bolometer data shows relatively less radiation loss near the X-point at this time compared to unpumped discharges. Continued neon puffing produced a steadily increasing neon concentration in the core plasma, and this affected the ELM behavior, as indicated by the divertor H_α emission (d). In fact, ELM activity is a sensitive indicator of impurity leakage from the divertor. Late in time, the power flow across the separatrix has been reduced to the point where only small, Type III ELMs are observed.

5. THE RADIATIVE DIVERTOR PROGRAM

We are now designing a new divertor structure scheduled to be installed at the end of 1996. This new divertor should increase the compatibility of radiative divertor operation with high confinement, high beta, non-inductive current drive plasmas. It (see Fig. 9) is designed to limit the escape of gas (fuel and impurities) from the divertor back to the core plasma by i) more closely matching the divertor surfaces to the magnetic flux surfaces of high triangularity double-null discharges, ii) providing pumping at both divertors in both the private region and at the outer strike point, and iii) enhancing recycling on the high heat flux surfaces by directing recycled neutrals preferentially inward toward the separatrix.

A key design parameter is the depth of the divertor slot required in this new configuration. Present experimental results show that large heat flux reductions can be obtained with divertor depths of 5–25 cm. Modeling confirms this [26]. Therefore, we concentrated on finding a divertor shape whose primary function would be to minimize the

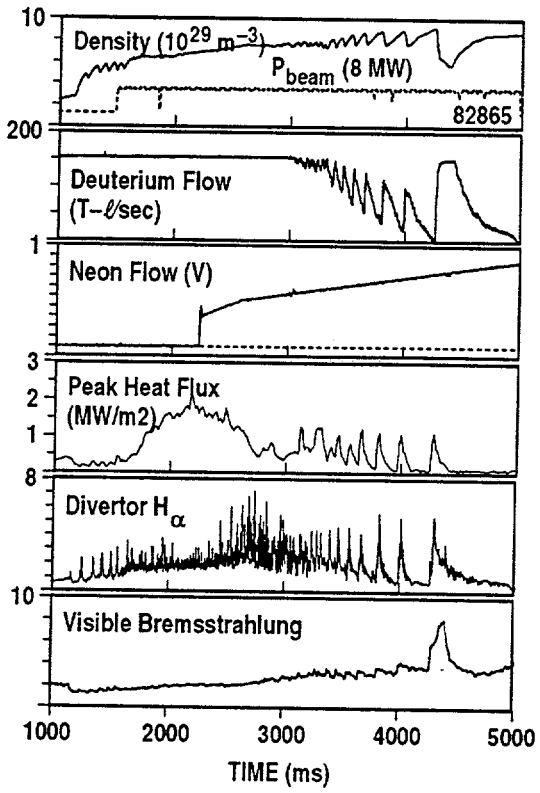

Fig. 8. Neon injection with D_2 injection and divertor pumping. (a) electron density and beam power (dashed), (b) deuterium flow rate, (c) particle exhaust rate, (d) neon flow, (e) peak divertor heat flux, (f) central visiible Bremsstrahlung signal normaized by T_e and $\bar{n}_e$

escape of neutrals from the divertor. This was explored using the DEGAS neutral transport code with a plasma model supplied by the UEDGE code. The modeling showed [27] that a 23 cm deep slot like that in Fig. 9 should reduce the fraction of neutrals escaping by a factor of 3–4 compared to the present open divertor configuration. While a deeper slot might reduce this still more, we found that controlling recycling at the top of the slot was more important, and so we shaped the baffle to gradually move out from the 1 cm to the 2 cm equivalent midplane magnetic flux surface. The design is flexible, however, so that the depth of the slot can be increased easily to 43 cm.

The installation of this new divertor hardware will impact the DIII–D program in several ways. Our divertor design matches the triangularity needed to obtain the best confinement and highest normalized beta. We will be able to pump these plasma to enable non-inductive current profile control. Capability for single-null divertor and low triangularity operation will be preserved, though at reduced parameters ($\kappa = 1.8$, $\delta = 0.8$, $I_p = 1.6$ MA). A number of divertor diagnostics will be modified to allow detailed studies to be carried out. However, the addition of the internal structure will make it possible to improve access in some cases, such as adding localized chords for divertor spectroscopy and bolometry.

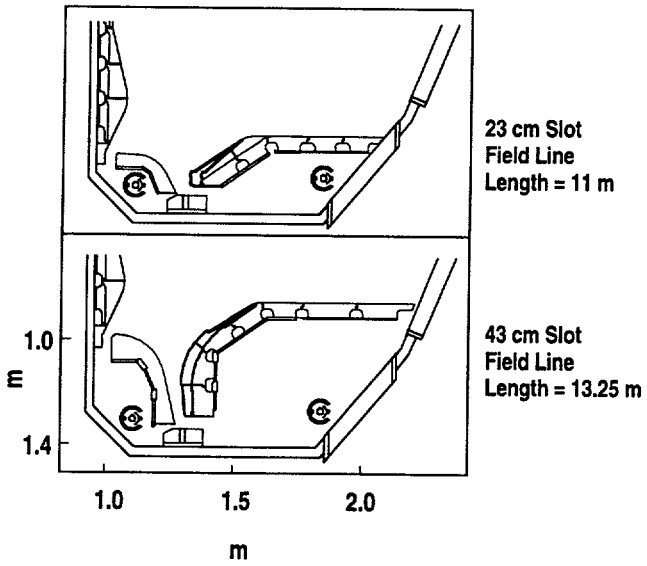

Fig. 9. Cross section of planned modification to DIII–D lower divertor as part of the Radiative Divertor Program. Upper divertor is identical.

6. SUMMARY AND CONCLUSIONS

In this paper we have reported on recent progress toward developing ITER and TPX-relevant divertors using the DIII–D tokamak. We have shown that divertor pumping can provide adequate particle exhaust for density control. Divertor pumping has also allowed us to maintain density control during D_2 puffing experiments with partially detached divertor plasmas and large reductions (3× or more) in peak divertor heat flux. We believe that the partially detached divertor plasma offers an attractive, naturally occurring way to reduce the divertor heat flux using little valuable space in the high field region, and that it is well matched to the high density operating point of the machine. Due to ITER's large size, radiative heat loads from an X-point Marfe in ITER could be maintained below 5 MW/m^2 with little more than 20 cm spacing to the nearest surfaces. The further advantage of this operating regime is that the ELM amplitude will be minimized, plasma cleanliness enhanced, and helium exhaust maintained

Our results with neon puffing are very similar to those reported by the TEXTOR group [28], and confirm that radiating mantles may also be applicable to ITER operating ELMing H–mode discharges at high density. In this case, however, feedback will be more important because of the strong coupling between edge radiation, ELM behavior, and impurity transport. Low density high power operation, such as that required for current drive in TPX, will be more problematic due to the larger edge concentrations required.

Using impurity injection to enhance mainly the divertor radiation still needs more study to determine its general feasibility, particularly for low density operation (below 60%–70% of the Greenwald limit). The ability of the scrape-off layer plasma to retain impurity ions and to keep neutrals from getting back to the main plasma is a limiting factor that is not well known. The extent to which divertor pumping and edge fueling can be used

to control the divertor conditions independently of the main plasma parameters has yet to be determined. New divertor hardware which improves the retention of impurities in the divertor will be tested in DIII–D in the near future, on a configuration that allows us to obtain high confinement and high β simultaneously with good divertor operation.

REFERENCES

[1] ITER Conceptual Design Report, ITER Document Ser. no. 18 (IAEA, Vienna, 1991), and TPX Physics Design Description, TPX Rep.ort 93-930325-PPPL, (PPPL, 1993)

[2] MAHDAVI, M.A., et al., in Proc. of the 20th Euro. Conf. on Contr. Fusion and Plasma Physics, Lisboa, Portugal, Vol. 17C, (European Physical Society, Petit-Lancy, Switzerland, 1993) p. 647.

[3] HILL, D.N., et al., in Plasma Phys. and Contr. Nucl. Fusion Research, Washington, D.C, 1990 (International Atomic Energy Agency, Vienna, 1991) Vol. 3, p. 487.

[4] ALLEN, S.L., et al., in Proc. of 11th Intnl Conf. on Plasma Surface Interactions, Mito, Japan, 1994, and General Atomics Report GA-A21714 (1994).

[5] SMITH, J.P, et al., Fusion Technol. **21** (1992) 1638; MENON, M.M., et al., Fusion Technol. **22** (1992) 356; SCHAUBEL, K., et. al., Proc. of 1993 Cryogenic Engineering Conference, Albuquerque, N.M., July 12–16, 1993.

[6] SCHAFFER, M.J., et al., Nucl. Fusion **32** (1992) 855.

[7] SCHISSEL, D.P, et al., General Atomics Report GA-A21621 (1994), submitted to Nucl. Fusion Letts.

[8] MAHDAVI, M.A., et al., in Proc. 16th Euro. Conf. on Contr. Fusion and Plasma Physics, Venice, Italy, Vol. 1, p. 249.

[9] SCHAFFER, M.J., et al., General Atomics Report GA-A21687, October 1994, submitted to Nucl. Fusion Letters.

[10] SCHAFFER, M.J., et al., to be submitted to Nucl. Fusion.

[11] WADE, M.R., et al., "Helium Exhaust Studies in ELMing H–Mode Discharges in the DIII–D Tokamak Using an Argon-Frosted Divertor Cryopump," General Atomics Report GA-A21652 (1994) to be published in Phys. Rev. Lett.

[12] ROGNLIEN, T.D., et al., J. Nucl. Mater. **196–198** (1992) 347 .

[13] PORTER, G.D., et al., these proceedings.

[14] LEONARD, A.W., et al., in Proc. of 10th Topical Conf. on High Temp. Plasma Diagnostics, Rochester, New York; General Atomics Report GA-A217033 (1994).

[15] LEONARD, A.W., et al., in Proc. of 11th Intnl Conf. on Plasma Surface Interactions, Mito, Japan, 1994; and General Atomics Report GA-A21693 (1994).

[16] HILL, D.N., et al., J. Nucl Mater. **176&177**, 158 (1990).

[17] MAINGI, R., et al., in Proc. of 11th Intnl Conf. on Plasma Surface Interactions, Mito, Japan, 1994; and General Atomics Report GA-A21705 (1994).

[18] MAHDAVI, M. A., et al., Phys. Rev. Lett. **47**, 1602 (1981).

[19] WEST, W.P., et al., General Atomics Rep. GA-A21762 (1994) and to be published in Proc. 21st. Euro. Conf. on Contr. Fusion and Plasma Physics.

[20] WATKINS, J.G., et al., in Proc. of 11th Int. Conf. on Plasma Surface Interactions, Mito, Japan, 1994; and General Atomics Report GA-A21708 (1994).

[21] EVANS, T.E., in Proc. of 11th Intnl Conf. on Plasma Surface Interactions, Mito, Japan, 1994, and General Atomics Report GA-A21707 (1994).

[22] PETRIE, T.W., et al., in Proc. 18th Euro. Conf. on Contr. Fusion and Plasma Physics, Berlin, Germany, Vol. 3, p. 237; PETRIE, T.W., et al. J. Nucl. Mater, **196–198** (1992) 848 .
[23] NEUHAUSER, J., et al., Nucl. Fusion **26** (1986) 1679.
[24] GHENDRIH, Ph., et al. in Proc. of 11th Intnl Conf. on Plasma Surface Interactions, Mito, Japan , 1994.
[25] SCHAFFER, M..J., et al., "Impurity Reduction During `Puff and Pump' Experiments on DIII–D," General Atomics Report GA-A21687, to be submitted to Nucl. Fusion Lett.
[26] SCHNEIDER, R. et al., in Proc. of 11th Intnl Conf. on Plasma Surface Interactions, Mito, Japan , 1994.
[27] FENSTERMACHER, M.E., et al., in Proc. of 11th Intnl Conf. on Plasma Surface Interactions, Mito, Japan , 1994.
[28] SAMM, U., et al., Plasma Phys. and Controlled Fusion **35** Suppl. (12)B (1993) B167.

ACKNOWLEDGMENTS

Work supported by the U.S. Department of Energy under Contract Nos. W-7405-ENG-48, DE-AC03-89ER51114, DE-AC05-84OR21400, DE-AC05-84OR21400, DEAC04-76DP00789, and Grant Nos. DE-FG03-89ER51121 and DE-FG03-86ER53225.